^{44}Ti: Its effective decay rate in young supernova remnants, and its abundance in Cas A

Y. Mochizuki[1], K. Takahashi[2], H.-Th. Janka[2], W. Hillebrandt[2], and R. Diehl[3]

[1] The Institute of Physical and Chemical Research (RIKEN), Hirosawa 2-1, Wako, Saitama 351-0198, Japan
[2] Max-Planck-Institut für Astrophysik, Karl-Schwarzschild-Straße 1, D-85740 Garching, Germany
[3] Max-Planck-Institut für Extraterrestrische Physik, Giessenbachstraße 1, D-85740 Garching, Germany

April 20, 1999

Abstract. Radioactive isotopes such as ^{44}Ti offer probably the most direct probe into nucleosynthesis environments in the interior of exploding stars, when the associated γ-ray activities in the explosion remnant are detected and translated back to the isotopic abundances at the time of the explosion. In this paper, we assert that the procedure may not necessarily be straightforward, at least in the case of ^{44}Ti, an orbital-electron capture decay isotope. Using the analytic model of McKee & Truelove (1995) for young supernova remnants, and assuming the existence of overdense ^{56}Fe-dominated clumps that contain also ^{44}Ti, we show that a high degree of ionization may be caused by the reverse shock so that the electron-capture rate of ^{44}Ti could be significantly reduced from its laboratory value. When applied to Cas A, this increases under certain conditions the current ^{44}Ti-activity by a factor $1.5 \sim 2.5$, which yields a better compatibility between the COMPTEL observation of the 1.16 MeV line activity associated with the ^{44}Ti decay and the SN model predictions of the initial ^{44}Ti abundance. This possibility is, however, subject to various uncertainties, and in particular to the unknown properties and radial distribution of the clumps in the ejecta.

Key words: supernovae: general – supernovae: individual: Cas A – ISM: supernovae remnants – Nuclear reactions, nucleosynthesis, abundances

1. Introduction

Exploding massive stars, and supernovae in particular, are known to be major sites for the production of a large variety of elements heavier than carbon. One of the few available ways to study the physics in the deep interior of such stars is the determination of the abundances of stable nuclides freshly produced and ejected by the explosion. Infrared, optical, and X-ray spectroscopic measurements are capable of determining elemental abundances in the photosphere during different phases of the outburst. But the results from such observations are, in general, sensitive to the models of line excitations in the photosphere, resulting in large correction factors to be applied before deducing the isotopic yields at the time of the explosion. In addition, results are hampered by the uncertainty of the optical depth, and by the possibility of heavy element condensation into dust shortly after the explosion, as was witnessed in SN 1987A.

A more direct probe of massive-star interior physics is, in principle, to investigate unstable nuclides and to measure the γ-rays associated with their β decays after they have been ejected by the supernova explosion. For an optimum probe, the mean lifetime of such a radioactive isotope should range from around a few weeks up to about 10^6 years. The lower limit is set by the requirement that the ejecta should become optically thin to γ-rays in a few decay times, and the upper limit by instrumental sensitivities of γ-ray telescopes (the γ-ray flux from a trace isotope must exceed the instrumental noise level, presently in the range of 10^{-5} photons cm^{-2}s^{-1}, which corresponds, for instance, to (several times) 10^{-2} M$_\odot$ of an intermediate-mass isotope with a lifetime of 10^6 y at the Galactic center or to 10^{-4} M$_\odot$ of the isotope in a supernova at a distance of a few hundreds of pc).

Furthermore, whereas short-lived isotopes will clearly trace individual events, long-lived ones with mean lifetimes of the order of 10^6 y or longer will reflect a superposition of different supernovae at different times, mixed with interstellar matter. Consequently clues to abundances in an individual object are only very indirect.

Only a few isotopes fulfill those constraints (see e.g. Diehl and Timmes 1998). Most promising cases are found among the Fe group elements, primarily because of their expected large abundances. The 0.847 and 1.238 MeV γ-

Send offprint requests to: Y. Mochizuki (motizuki@postman.riken.go.jp)

ray lines from the ^{56}Co $\rightarrow^{56}$Fe decay (half-life: $t_{1/2} = 77$ d) were detected from SN 1987A (Matz et al. 1988; Sandie et al. 1988; Mahoney et al. 1988; Rester et al. 1988; Teegarden et al. 1989). There is also evidence for these decay lines from the unusually fast and bright Type Ia supernova 1991T (Morris et al. 1995, 1997). The ^{57}Co $\rightarrow^{57}$Fe decay ($t_{1/2} = 272$ d) is another probe: the 122 and 136 keV lines were detected from SN 1987A (Kurfess et al. 1992; Clayton et al. 1992). Cases at the upper end of the favored radioactive lifetime range are ^{26}Al ($t_{1/2} = 7.4 \times 10^5$ y) and ^{60}Fe ($t_{1/2} = 1.5 \times 10^6$ y). The 1.809 MeV line from the ^{26}Al decay has been detected and mapped along the entire plane of the Galaxy (see review by Prantzos & Diehl 1996). If supernovae, rather than Wolf Rayet stars, were responsible for this ^{26}Al, the lines from the ^{60}Fe β^- decay would be expected simultaneously with the ^{26}Al decay, identifying a supernova origin (review by Diehl and Timmes 1998). Instrumental sensitivity appears just at the borderline for this test.

In this paper, we focus our discussion on ^{44}Ti, which decays with $t_{1/2} = 60$ y (Ahmad et al. 1998; Görres et al. 1998; Norman et al. 1998; Wietfeldt et al. 1999), making it ideal for a study of inner-supernova physics within young supernova remnants. ^{44}Ti decays almost uniquely to the 2^{nd} excited state of ^{44}Sc, followed immediately by the almost unique β^+ decay of ^{44}Sc ($t_{1/2} = 4$ h) to the 1.156 MeV excited state of ^{44}Ca. The 1.156 MeV de-excitation line has indeed been observed by the COMPTEL telescope on the Compton Observatory from Cas A, a young supernova remnant with an estimated age of 320 y (Iyudin et al. 1994, 1997; Dupraz et al. 1997). The measured γ-ray flux is $\simeq (4 \pm 1) \times 10^{-5}$ photons /cm^2/s (Iyudin et al. 1997) concordant with an upper limit obtained by the OSSE instrument (The et al. 1996). With an adopted distance to Cas A of 3.4 kpc (Reed et al. 1995) and the laboratory decay rate, the inferred initial mass of ^{44}Ti is $\simeq 2 \times 10^{-4}$ M$_\odot$ (Iyudin et al. 1997; Woosley & Diehl 1998).

The current model predictions of the ^{44}Ti initial mass lie in an approximate range of $(6 \times 10^{-6} \sim 8 \times 10^{-5})$ M$_\odot$ for Type-II SNe (Woosley & Weaver 1995; Thielemann et al. 1996), and of $(3 \sim 8) \times 10^{-5}$ M$_\odot$ for Type-Ib SNe (Woosley et al. 1995), more or less strongly depending on the progenitor masses. Higher values up to 2×10^{-4} M$_\odot$ were obtained in some of the Type-II SN models, when progenitor masses above 30 M$_\odot$ combine with high explosion energies (Woosley & Weaver 1995), and for a 20 M$_\odot$ (SN1987A) model star (Thielemann et al. 1996). Barring the possibility that the progenitor of Cas A happened to be such a star, one may conclude that COMPTEL observed significantly more ^{44}Ti than expected (see, e.g., Fesen & Becker 1991; Hurford & Fesen 1996 for discussions on the progenitor characteristics).

As far as its β-decay properties are concerned, ^{44}Ti is a very interesting trace isotope, because its decay mode is pure orbital electron capture, which means that fully ionized ^{44}Ti is stable. Even partial ionization of the innermost electrons should lead to a considerably longer effective half-life (Mochizuki 1999). Therefore, the question arises whether in supernova remnants ^{44}Ti could be highly ionized and thus more stable for a considerable period of time during the evolution. In this case, it would be incorrect to use the half-life measured in the laboratory, and initial abundances of ^{44}Ti as deduced from γ-ray intensities could be too high.

However, there is no simple answer to this question and, as we shall emphasize below, the thermodynamic history of a remnant has to be known in detail before firm predictions can be made. On the other hand, it is interesting to speculate whether the COMPTEL observations, which indicate an amount of ^{44}Ti in Cas A that appears higher than expected, reflect the effects of an increased lifetime of the explosively-produced ^{44}Ti because of temporary and partial ionization.

The primary aim of the present paper is to outline possible implications of (partial) ionization on the observable γ-ray line flux from the decay of ^{44}Ti. We shall present results obtained for a variety of different conditions, based on a simple model for young supernova remnants which, nonetheless, accounts for the features most relevant to this question. Of course, our main focus will be on Cas A, the best studied case, and the parameters of the model are chosen accordingly.

Section 2 contains an overview of observational aspects of SN explosions and remnants which are of relevance in the context of this work. In Sect. 3, we describe the employed model for young supernova remnants, i.e., the analytic model of McKee & Truelove (1995), augmented by a description of the reverse shock interacting with denser cloudlets (Sgro 1973; Miyata 1996). In addition, we describe the microphysics used in the model on which the calculation of the "effective" decay rate of ^{44}Ti is based. In Sect. 4, we present our results for the time variation of the ^{44}Ti decay rate, the ^{44}Ti abundance in young supernova remnants and the associated γ-ray activities that can be measured. As a specific example, we will preferentially use the case of Cas A. Summary and conclusions are given in Sect. 5.

2. Young Supernova Remnants

Studies of supernovae from the moment of the explosion up until they dissolve and merge with the general interstellar medium has, in general, been guided by observational opportunities as combined with model interpretations; the interplay of different physical processes, which vary spatially and rapidly within a young supernova remnant, cannot be disentangled from measurements alone. Observational windows are (from low to high energy radiation): Radio maps from electrons synchrotron-emitting in magnetic-field structures around the shocked-gas region; infrared emission from cool and hot dust within dense clumps embedded in the supernova remnant; optical line emission from the edges of dense material embedded in the remnant's hot plasma; X-ray emission from the hot, ionized, gas that has been shocked by the forward blast wave and by the reverse shock traveling inward, respectively; and γ-rays from long-lived radioactivity such as ^{44}Ti.

Here we are mainly interested in the thermal history of the radioactive ^{44}Ti after it has been ejected in a supernova explosion. ^{44}Ti as well as other iron-group elements are synthesized during the very early moments of the explosion of a massive star in the layers adjacent to the nascent compact object (a neutron star or black hole). Therefore, observations of iron can be used to trace also ^{44}Ti. However, not many good cases are known so far.

SN 1987A is certainly the best studied case. The large Doppler shifts of iron lines observed in the early spectra require that iron moves with velocities much higher than some of the hydrogen which cannot be explained by spherically symmetric explosion models but indicates that it is not homogeneously distributed in an expanding shell but is found in clumpy structures. This conclusion is also supported by the unexpectedly early detection of X- and γ-rays from the decay of radioactive elements (for summaries, see Woosley & Weaver 1994, Nomoto et al. 1994), which again suggests that these nuclei have been transported far out into the hydrogen-rich shells. Other arguments in favor of this interpretation include the smoothness of the light-curve (e.g., Woosley & Weaver 1994, Nomoto et al. 1994 and references therein), and the time-dependent features of the spectral lines observed soon after the outburst (Utrobin et al. 1995), e.g., in the Bochum event (Hanuschik & Dachs 1987; Phillips & Heathcote 1989). In fact multi-dimensional supernova simulations (e.g., Herant et al. 1992, 1994; Shimizu et al. 1994; Shimizu 1995; Burrows et al. 1995; Janka & Müller 1995, 1996) have demonstrated that the surroundings of the newly-formed neutron star are stirred by hydrodynamic instabilities and that inhomogeneities and clumpiness of the products of explosive nucleosynthesis are likely the consequence. However, it cannot be excluded that SN 1987A is a special case and not comparable with, e.g., Cas A.

^{44}Ti γ-ray emission is expected from core-collapse supernovae in general (e.g., Woosley & Weaver 1995; Thielemann et al. 1996), yet there is a significant deficit in such γ-ray line sources in the Galaxy for the inferred Galactic core-collapse supernova rate (Dupraz et al. 1997). The ^{44}Ti detection for Cas A (Iyudin et al. 1994; 1997), despite the low Fe abundance, therefore has given rise to speculations about its exceptional nature, particularly because its optical and X-ray characteristics support the idea of asymmetries and a peculiar circumstellar environment (see below, and Hartmann et al. 1997 and references therein). It was suggested, for example, that the progenitor of Cas A might have been a rapidly spinning star, in which case more ^{44}Ti could have been synthesized (Nagataki et al. 1998).

Recently, a second Galactic ^{44}Ti source has been reported (Iyudin et al. 1998). Its alignment with an also recently discovered X-ray remnant (Aschenbach 1998) suggests that it is a very young and most nearby supernova remnant, with an age around 680y and a distance of 200pc only. This object still provides a puzzle because of the absence of radio and optical emission expected for such a nearby supernova. Yet, if confirmed, it will provide a unique opportunity for the study of supernova-produced ^{44}Ti; in which case it is of some interest to see if the modified decay rate of ionized ^{44}Ti addressed in our paper could also be important.

The ^{44}Ti found in young supernova remnants is probably formed during the α-rich freezeout from (near) nuclear statistical equilibrium (Woosley et al. 1973; Woosley & Weaver 1995; Woosley et al. 1995; Thielemann et al. 1996; Timmes et al. 1996; Timmes & Woosley 1997; The et al. 1998). Whereas ^{44}Ti is obviously fully ionized at the time of explosion, ^{44}Ti ions will recombine with electrons during the adiabatic cooling phase, which accompanies the expansion of the exploded star, to become neutral after some 1000 s (e.g., Nomoto et al. 1994), a negligible timescale when compared with the age of a supernova remnant. Therefore, during most of this early phase ^{44}Ti will decay with the laboratory rate. The subsequent evolution of the remnant may however provide conditions for its reionization, which is the subject of our modeling effort.

The evolution of young supernova remnants has been modeled extensively, and the spherically-symmetric explosion into homogeneous interstellar surroundings appears well-understood (McKee and Truelove 1995). A free expansion phase is followed by an adiabatic blast-wave phase, where interaction with surrounding material produces outward and inward moving shock waves leading to bright X-ray and radio emission, yet being unimportant for the energetics of the remnant. Later phases of significant slowing-down and radiative losses of the expanding remnant lie beyond the early phase where ^{44}Ti still decays. Young remnants such as Cas A are generally understood as being somewhere intermediate between free expansion and the second phase, commonly called "Sedov-Taylor" phase.

The evolution of such idealized young supernova remnants during the ejecta-dominated stage ($t < t_{\rm ST}$) and the Sedov-Taylor phase ($t > t_{\rm ST}$) was described in an analytical model by McKee & Truelove (1995). At the interface between ejecta and ambient medium a contact discontinuity occurs, separating the exterior region of shocked and swept-up circumstellar gas behind the outward-moving blastwave from the supernova remnant interior. Inward from the discontinuity, a reverse shock travels through the expanding, cold supernova ejecta, heating up the interior gas. Bright X-ray emission results from the hot plasma on both sides of the contact discontinuity, with higher temperature on the outside heated by the blastwave ($\geq$ keV), as compared with reverse-shock heated gas on the inside ($\leq$ keV; e.g. Vink et al. 1996). Although such a two-temperature model appears adequate to describe the X-ray emission of many supernova remnants, considerable uncertainty remains in detail. For example, the blastwave shock rapidly heats the ions entering the blastwave region, the thermalization times for the X-ray emitting electrons may exceed 100 years, so that non-equilibrium models are needed for a proper description of X-ray and radio emission. The detailed physical conditions within supernova remnants are far from being understood, although the general evolution follows these fairly simple descriptions quite closely, and is controlled by a few parameters, the explosion energy, the mass of ejecta, and the surrounding medium density. According to the McKee & Truelove (1995) model, an explosion energy in the $(1 \sim 3) \times 10^{51}$ erg range does not seem unreasonable in the case of Cas A for the possible ejecta mass of $(2 \sim 5)$ $M_{\odot}$ (Tsunemi et al. 1986; Vink et al. 1996) if the surrounding ambient gas density is of the order of 20 cm^{-3} (Tsunemi et al. 1986) and the current blastwave radius is $(2 \sim 3)$ pc for an assumed distance of 3.4 kpc (Anderson & Rudnick 1995; Holt et al. 1994; Jansen et al. 1988; Reed et al. 1995).

Although the general appearance of supernova remnant images in the radio and in X-rays is that of a large-scale shell configuration as expected from the above model, additional prominent clumpy structures appear in some cases (e.g., Anderson & Rudnick 1995; Koralesky et al. 1998). This suggests that the model outlined so far is an oversimplification as far as details are concerned. The gross radio and X-ray emissivity may not be very sensitive to such discrepancy, tracing the electron component in the vicinity of the shock region, but the bulk ejected mass may be inadequately represented by the inferred electron densities and temperatures (e.g., Koralesky et al. 1998). Thus, for the Cas A remnant, prominent structures have been studied in their respective forms of optical knots and filaments, "quasi-stationary flocculi", "fast-moving knots", and "fast-moving flocculi" (e.g., van den Bergh & Kamper 1983; Reed et al. 1995; Peimbert & van den Bergh 1971; Chevalier & Kirshner 1977, 1978, 1979; Reynoso et al. 1997; Lagage et al. 1996). There is overwhelming evidence for dense structures embedded in tenuous material within the entire remnant, and even outside the blastwave shock radius. Obviously the explosion itself produces fragments of material, seen now as fast-moving knots with their abundance patterns supporting an ejecta origin. These clumps might carry heavier elements preferentially as suggested by observations of fast-moving Fe clumps early in SN explosions, e.g. in SN 1987A (e.g., Nomoto et al. 1994, Wooden 1997 and references therein), but a connection between the instabilities and clumpiness early after the supernova explosion and the fragments and "bullets" seen in the remnants has not been established yet.

Given all these uncertainties in the evolution of supernova remnants we do not attempt to model a specific object, such as Cas A, in detail here. We rather shall investigate by means of an admittedly very simple model, varying its parameters within reasonable limits, the potential effects of ionization on the ^{44}Ti abundance estimates obtained from γ-ray observations.

3. The Model

The remnant model employed in this work uses the analytic description by McKee & Truelove (1995) for the hydrodynamic evolution. The ejecta with mass $M_{\rm ej}$ are assumed to be cold and to expand with explosion energy $E_{\rm ej}$ into a homogeneous ambient medium which has a hydrogen number density $n_{\rm H0}$ and is composed of 10 hydrogen atoms per helium atom, corresponding to a helium mass fraction of 28.6%. Inside the homogeneous ejecta, we assume the existence of denser clumps that contain a small fraction of the ejecta mass but most of the produced ^{44}Ti. The treatment of the interaction of the reverse shock with these clumps and of the corresponding effects on the ^{44}Ti decay are described below. Ionization of ^{44}Ti is most efficiently induced by electrons. If and how long a high degree of ionization is sustained depends on the reverse-shock characteristics and the postshock evolution of the matter containing ^{44}Ti.

3.1. A model for young supernova remnants

If sufficiently high temperatures happen to be reached behind the reverse shock, ^{44}Ti may become fully ionized, in which case its decay is prevented until cooling due to the expansion of the gas leads to (partial) recombination of the innermost electrons.

To follow the radioactivity of the supernova remnant requires knowledge of the evolution of the shocked ejecta. The analytical model of McKee & Truelove (1995) yields scaled relations for the radius, velocity and postshock temperature of the reverse shock as functions of time t. Also, the model provides the density of the unshocked (homogeneous) ejecta at time t, which allows one to calculate the postshock density from the density jump at the reverse shock. In order to describe the density history of each mass shell after the reverse shock has passed through it, we assume that the shocked matter moves (approximately) with the same velocity as the contact discontinuity. Knowing the motion of the latter, therefore, we can estimate the dilution of the shocked gas by the expansion of the supernova ejecta.

The time-dependent analytical solutions are given by the three parameters, $M_{\rm ej}$, $E_{\rm ej}$ and $n_{\rm H0}$. A combination of values of these parameters is considered to yield a suitable description of a certain supernova remnant, if the model gives a present-day radius and velocity of the blastwave that is compatible with observational data.

We extended the analytic remnant model of McKee & Truelove (1995) by assuming that the iron-group elements together with the explosively nucleosynthesized ^{44}Ti are concentrated in overdense clumps of gas. These clumps are assumed to move outward through the dominant mass of homogeneous supernova ejecta with high velocity. Since the clumps should contain only a minor fraction of the total mass of the ejecta, the dynamics of the young supernova remnant as described by the McKee & Truelove (1995) model is assumed not to be altered by their presence. The radial position r of the iron clumps within the ejecta can be measured by the relative mass coordinate q which is defined as

$$q \equiv \frac{4\pi r^3 \rho_{\rm ej}}{3\, M_{\rm ej}}\,, \tag{1}$$

where $\rho_{\rm ej}$ is the uniform background density of the ejecta which expand homogeneously.

3.2. Thermodynamic conditions just behind the reverse shock

We now consider the properties of a clump of metal-rich matter within the homogeneous ejecta. Denoting the density enhancement factor of the assumed clump relative to the surrounding ejecta by $\alpha_{\rm clmp}$, we obtain the clump density after the reverse shock has passed at time $t_{\rm sh}$ as

$$\rho(t_{\rm sh}) = 4\,\alpha_{\rm clmp}\,\rho_{\rm ej}(t_{\rm sh})\,, \tag{2}$$

for an adiabatic index $\gamma = 5/3$.

Correspondingly, the post-reverse shock temperature of the clump is related to that of the surrounding uniform ejecta, $T_{\rm ej}(t_{\rm sh})$, as

$$T(t_{\rm sh}) = \frac{\beta(\alpha_{\rm clmp})}{\alpha_{\rm clmp}}\,\frac{\mu(t_{\rm sh})}{\mu_{\rm ej}}\,T_{\rm ej}(t_{\rm sh})\,, \tag{3}$$

which generalizes by the factor $\mu(t_{\rm sh})/\mu_{\rm ej}$ the result of Sgro (1975) to the case considered here, where the chemical composition of the clump is different from that of the surrounding ejecta as described by the corresponding mean molecular weights $\mu(t_{\rm sh})$ and $\mu_{\rm ej}$, respectively. $T_{\rm ej}(t_{\rm sh})$ is given by

$$T_{\rm ej}(t_{\rm sh}) = \frac{3\mu_{\rm ej}}{16k}\,\widetilde{v}_{\rm r}^{\,2}(t_{\rm sh})\,, \tag{4}$$

where $\widetilde{v}_{\rm r}$ is the reverse-shock velocity in the rest frame of the unshocked ejecta (McKee & Truelove 1995). In Eq. (3), β is the ratio of the pressure values in the regions behind the reflected shock and in front of it. The reflected shock is formed when the reverse shock hits a dense clump in the ejecta (Sgro 1975; Miyata 1996). The ratio β is related to $\alpha_{\rm clmp}$ as

$$\alpha_{\rm clmp} = \beta\left(1 + \frac{1-\beta}{\sqrt{4\beta+1}}\right)^{-2}, \tag{5}$$

for $\gamma = 5/3$ (Sgro 1975). In particular, $\beta = 1$ if $\alpha_{\rm clmp} = 1$ (no clumpiness), and $\beta/\alpha_{\rm clmp}$ appearing in Eq. (3) is less than unity for $\alpha_{\rm clmp} > 1$.

3.3. Post reverse-shock evolution

We now follow the fate of the homogeneous ejecta and of the matter in clumps after they have experienced the impact of the the reverse shock at time $t_{\rm sh}$. As we have mentioned earlier, we assume that the shock itself would continue to proceed inward through the cold ejecta as prescribed by the McKee & Truelove (1995) model. The thermodynamic and chemical evolution of the clumps at times $t \geq t_{\rm sh}$ is treated as described below.

Since we trace the clump material, it is preferable to introduce Lagrangian particle abundances, defined by

$$n \equiv \frac{{\rm d}N}{{\rm d}q}\,, \tag{6}$$

where dN is the number of particles at the mass coordinate q in the interval dq.

3.3.1. Ionic abundances

At a given time $t(\geq t_{\rm sh})$, the number abundance n_i of a nuclear species k with charge Z and i orbital electrons (i.e. $Z - i$ times ionized, and $n_k = \sum_{i\geq 0} n_i$) follows

$$\frac{{\rm d}n_i}{{\rm d}t} = -[\lambda_{\beta,i} + \lambda_{{\rm ion},i} + \lambda_{{\rm rec},i}]n_i + \lambda_{{\rm ion},i+1}n_{i+1} + \lambda_{{\rm rec},i-1}n_{i-1}\,, \tag{7}$$

where $\lambda_{\beta,i}(t), \lambda_{{\rm ion},i}(t)$, and $\lambda_{{\rm rec},i}(t)$ are the nuclear β-decay, ionization and recombination rates, respectively, of the ion. For ^{44}Ti, $\lambda_\beta \neq 0$, and thus $n(t > t_{\rm sh}) < n(t_{\rm sh}) = n(0){\rm exp}(-\lambda_{\rm lab} t_{\rm sh})$, where $\lambda_{\rm lab}$ is the ^{44}Ti decay rate in the cold ejecta, i.e. its laboratory value.

Since we assume that material which contains ^{44}Ti consists dominantly of one single stable nuclide (^{56}Fe in practice), the number of ionization electrons, $n_{\rm e}$, is given by $\sum_{i\geq 0}(Z-i)n_i$ for that species. In practice, we further assume that both ^{56}Fe and ^{44}Ti are ionized to some degree in the reverse shock itself, which we cannot resolve. Typically, we start our network calculations with ionic systems of 10 bound electrons, This choice is made since our major concern is to see the reduction of the orbital-electron capture rates in the domains of high shock temperatures.

The reaction rates entering in Eq. (7) are discussed in Appendix A.

3.3.2. Ion and electron temperatures

The network requires the knowledge of the thermodynamic evolution of the shocked matter, and in particular of the electron temperature, $T_{\rm e}$, which defines the Boltzmann distribution, and of the matter density ρ (or the ion number density, $n_{\rm ion}$), which enters in the absolute electron number density $n_{\rm e}$.

The decrease by expansion of the temperature $T(t)$ from $T(t_{\rm sh})$ of Eq. (3) would roughly be proportional to

$[\rho(t)/\rho(t_{\rm sh})]^{2/3}$ (for $\gamma = 3/5$ and $t > t_{\rm sh}$). Two considerations are due, however. One concerns the possibility that both $T_{\rm e}$ and the ion temperature, $T_{\rm ion}$, may not necessarily be the same as T. Secondly, some non-adiabatic effects may appear as the result of ionization and recombination.

It is sometimes asserted that the collisionless equilibration between $T_{\rm ion}$ and $T_{\rm e}$ would occur quickly, in which case $T_{\rm ion} = T_{\rm e} = T$ already at $t = t_{\rm sh}$. Save this possibility, the equipartition of the shock energy to ions and electrons may not be achieved at once. The equilibration process through the Coulomb interaction is described by a non-linear equation (Spitzer 1962),

$$\frac{{\rm d}T_{\rm e}}{{\rm d}t} = \frac{T_{\rm ion} - T_{\rm e}}{\tau_{\rm eq}}, \tag{8}$$

in terms of the equilibration time $\tau_{\rm eq}(t)$, which is a function primarily of $T_{\rm ion}$, $T_{\rm e}$ and the number densities of ions and electrons. Assuming that $T_{\rm e} \ll T_{\rm ion}$ at $t = t_{\rm sh}$, and that the total kinetic energy

$$\frac{3}{2}(n_{\rm ion} + n_{\rm e})T = \frac{3}{2}(n_{\rm ion}T_{\rm ion} + n_{\rm e}T_{\rm e}) \tag{9}$$

is constant during a short time interval δt, we solve Eq. (8) simultaneously with the abundance network equations to determine the degree of ionization of a dominant species, and thus $n_{\rm e}$.

In order to include the non-adiabatic effect caused by ionization and recombination, we assume that the energy required for unbinding additional electrons (net energy loss) is taken from electrons only. Namely, after performing the network calculation at each time step and solving Eq. (8), we make a replacement

$$T_{\rm e} \to T_{\rm e}\exp\left(-\frac{\delta n_{\rm e}}{n_{\rm e}} - \frac{2}{3}\frac{\delta Q}{n_{\rm e}T_{\rm e}}\right), \tag{10}$$

where $\delta n_{\rm e}$ and δQ are the change of $n_{\rm e}$ during δt and the corresponding net energy consumption. The equilibrium temperature T is then calculated from Eq. (9).

Finally, $T(t+\delta t), T_{\rm ion}(t+\delta t)$, and $T_{\rm e}(t+\delta t)$ are obtained from the current values by multiplying $[\rho(t+\delta t)/\rho(t)]^{2/3}$.

4. Results

We present here our results, which we obtained with the model described above. They depend on the following parameters: $E_{\rm ej}, M_{\rm ej}, n_{\rm H0}$, $\alpha_{\rm clmp}$ and two values for q, given as q_0 and q_1, which define the lower and upper boundaries of the mass shell where the ^{44}Ti-containing clumps are assumed to exist. As we mentioned earlier, the values of the first three can be constrained in the case of Cas A from the observational analyses of the blast-wave radius $R_{\rm b}$ and velocity $v_{\rm b}$. Below we consider mainly the parameter space which is consistent with these constraints. While we treat $\alpha_{\rm clmp}$ as a free parameter, a value of the order of 10 seems to be reasonable as a first guess, based on the density contrast which develops in hydrodynamic instabilities in the envelope of the progenitor star during the supernova explosion (Fryxell et al. 1991).

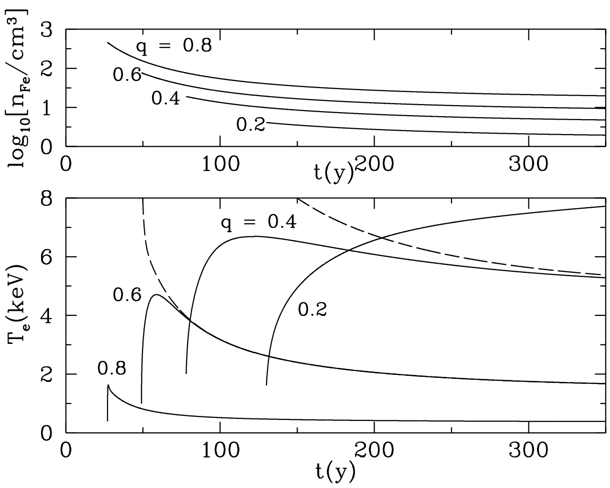

Fig. 1. Examples for the evolution with time t (in years) of the ^{56}Fe number density $n_{\rm Fe}$ (*top*), and of the electron temperature $T_{\rm e}$ (*bottom*) in the ^{56}Fe-dominated clumps at four different locations indicated by the mass coordinate q. The dashed lines represent the asymptotic behavior of the equilibrium temperatures $T(t)$ (as described in Sect. 3.3.2) at $q = 0.4$ and 0.6. The left edge of each solid curve corresponds to $t = t_{\rm sh}$. For example, the reverse shock took 50 y to reach $q = 0.6$. The results are given for the following set of parameter values: $E_{\rm ej} = 3 \times 10^{51}$ erg, $M_{\rm ej} = 3$ $M_\odot$, $n_{\rm H0} = 15$ cm^{-3} and $\alpha_{\rm clmp} = 10$

4.1. Thermodynamic evolution of post-shock clumps

Figure 1 shows the evolution of the ^{56}Fe number density $n_{\rm Fe}$ and of the electron temperature $T_{\rm e}$ in the ^{56}Fe-dominated clumps at four different locations in the ejecta, given by the corresponding mass coordinate q, after the reverse shock has passed the clumps. The post-shock expansion decreases the density as well as the equilibrium temperature, while $T_{\rm e}$ first increases in its attempt to reach equilibrium between electrons and ions. The results are plotted for the chosen set of parameter values quoted therewith.

4.2. *Effective decay rates of* ^{44}Ti *and its radioactivity as an observable*

Let us now consider ^{44}Ti in a clump that is located anywhere in the mass coordinate $0 \le q \le 1$ of the ejecta. If ^{44}Ti is near the surface (large q), it suffers from the reverse shock early. Since the electron temperature is still relatively low (see Fig. 1), there is no possibility to reach a high degree of ionization (thus an appreciable reduction of the decay rate). On the other hand, ^{44}Ti embedded in clumps located in the innermost region may become highly

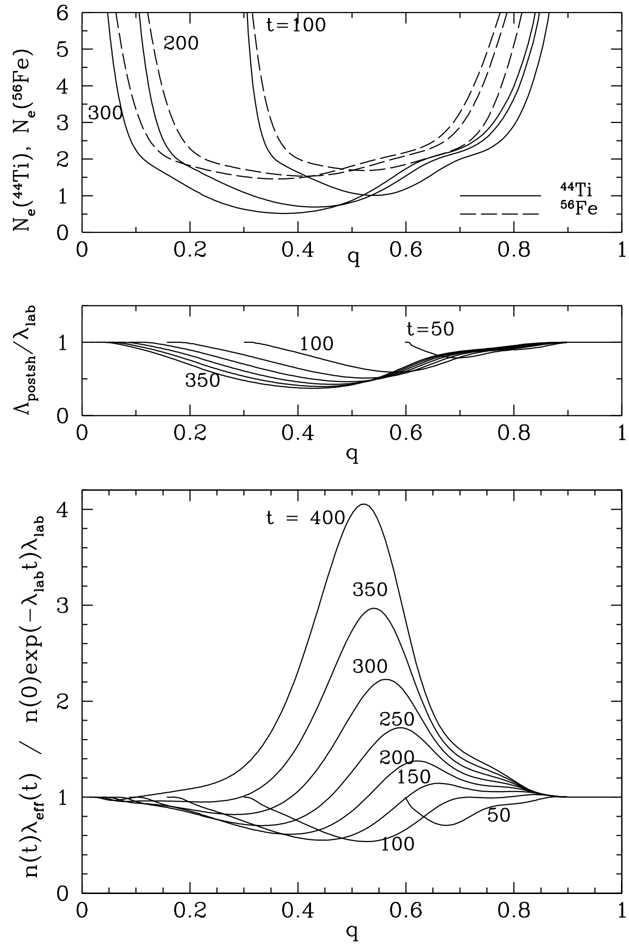

Fig. 2. *Top panel:* The average numbers N_e of electrons that are bound to ^{44}Ti and to ^{56}Fe at mass coordinate q and at time t (in y) after the explosion. *Middle:* Effective decay rates Λ_{postsh} of the shocked ^{44}Ti during the time span between t_{sh} and t [Eq. (11)] in units of the laboratory rate λ_{lab}. *Bottom:* The corresponding ^{44}Ti radioactivity observable at time t ("age") relative to the case that assumes no reduction of the β-decay rate. The parameter values used here are the same as those for Fig. 1

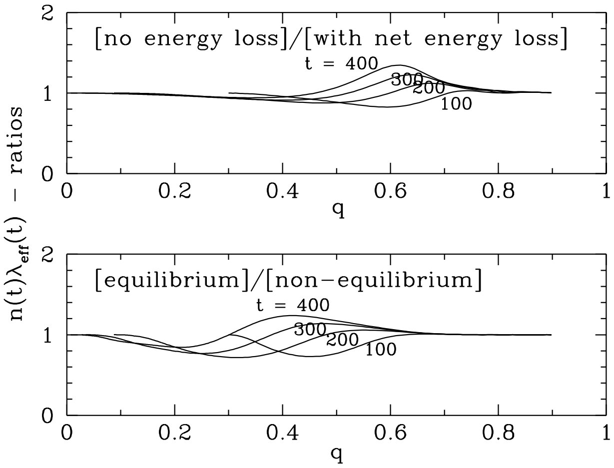

Fig. 3. ^{44}Ti radioactivities at times t (in y) in the clumps located at radial positions q, relative to the radioactivity of the model with most detailed input physics, when the non-adiabaticity of the thermal evolution of the clumps is ignored (*upper panel*) and when instantaneous equilibration between T_e and T_{ion} (toward T) is assumed (*lower panel*)

ionized as the temperature is generally highest, resulting in the smallest ^{44}Ti decay rate. Since t_{sh} is closer to t, the "age" of the remnant, however, the net effect of the reduced decay rate appears weaker. Therefore, the maximum effect of the retarded β-decay is obtained if ^{44}Ti is at intermediate values of q. This situation is depicted in the panels of Fig. 2.

The top panel of Fig. 2 shows the average numbers of electrons that are bound to ^{44}Ti and to ^{56}Fe at $t = 100, 200$ and 300 years after the explosion. The increase of N_e toward the low side of q indicates that the time span between t_{sh} and t was not long enough for ionization. At the high end of q-values, the effects of post-shock recombination are visible. When combined with n_{Fe} from Fig. 1, $N_e(^{56}Fe)$ determines the total number of ionization electrons, $n_e(t)$, in a clump: $n_e = [Z - N_e(^{56}Fe)]\ n_{Fe}$ with $Z = 26$.

The retardation of the ^{44}Ti decay by ionization is illustrated in the middle panel of Fig. 2. The effective decay rate in the post-shock period, Λ_{postsh}, is defined as the time-average of λ_{eff} [given by Eq. (18) in Appendix A] between the time t_{sh} and a time $t > t_{sh}$. It can be expressed as

$$\Lambda_{postsh} \equiv -\frac{1}{t - t_{sh}} \ln\Big[\frac{n(t)}{n(t_{sh})}\Big] , \tag{11}$$

where $n(t)$ is the ^{44}Ti abundance at mass coordinate q and time (age) t, and $n(t_{sh})$ is the corresponding value at the shock impact time t_{sh}, which has been reduced from its initial value $n(0)$ according to $n(t_{sh}) = n(0)\exp(-\lambda_{lab} t_{sh})$.

In order to estimate the observable consequences of the reduced β-decay rates, one has to recall that the measurable γ-ray activity per (normalized) unit mass of the remnant is the product of the current β-decay rate and the current abundance, $n(t)\lambda_{eff}(t)$. This introduces a nonlinear relation between the observable activity given in the bottom panel of Fig. 2 and the effective decay rates displayed above, particularly in the absence of quick recombination.

In Fig. 3, we compare the results obtained with the input physics as described in Sect. 3 to the cases where either the non-adiabaticity of the equilibration process of electrons and ions owing to the energy consumption by the ionization process is neglected (*upper panel*), or where instantaneous equilibration (i.e., $T_e = T_{ion} = T$ always) is assumed (*lower panel*). It can be seen that in both cases the trends of the "full" model shown in Fig. 2, where both the non-adiabaticity and the gradual equilibration process are taken into account, are somewhat enhanced. This can be understood by the fact that the omission of either of the two effects leads to higher electron temperatures and thus to a higher degree of ionization in the clumps.

4.3. ^{44}Ti *radioactivity in Cas A*

The ^{44}Ti radioactivity of the whole supernova remnant as observable at an age t, relative to the activity level that would result in the absence of any retardation of the β-decay rate by ionization, is defined by the ratio

$$\mathcal{A} \equiv \int_{q_0}^{q_1} n(q,t)\lambda_{\rm eff}(q,t)\mathrm{d}q \Big/ \Big[N(0)\exp(-\lambda_{\rm lab}t)\lambda_{\rm lab}\Big] . \quad (12)$$

Here, $N(0)$ is the total number of ^{44}Ti nuclei in the ^{56}Fe clumps at $t = 0$. For a remnant like Cas A, which is in the transition phase from the ejecta-dominated stage to the Sedov-Taylor phase, the reverse shock has passed through most of the ejecta. Therefore, the factor $\mathcal{A}$ must be expected to be larger than unity when the remnant is observed at this stage of its evolution. This implies that the initial abundance inferred from the current γ-ray activity due to the ^{44}Ti decay is lower by a factor $\mathcal{A}^{-1}$ than the amount of produced ^{44}Ti that is estimated on the basis of the laboratory decay rate $\lambda_{\rm lab}$.

For certain combinations of the characterizing parameters of the supernova remnant model, $E_{\rm ej}$, $M_{\rm ej}$ and $n_{\rm H0}$, the delayed decay of ionized ^{44}Ti can have a sizable effect on the γ-ray activity of Cas A which is observable at the present age of about 320 years. In Tables 1–3 the ratio $\mathcal{A}$ denotes the currently observable activity according to our model, normalized to the expected activity if ionization effects are not taken into account. The results depend on the assumed density enhancement $\alpha_{\rm clmp}$ in the clumps relative to the density of the homogeneous ejecta, and on the location of the clumps within a shell in the expanding ejecta bounded by the lower and upper mass coordinates q_0 and q_1, respectively. In addition, in Tables 1–3 numbers are given for the blast-wave radius $R_{\rm b}$ and the blast-wave velocity $v_{\rm b}$ as predicted by the McKee & Truelove (1995) model at the current age of the Cas A supernova remnant.

The ratio $\mathcal{A}$ exhibits the following tendencies. For fixed explosion energy and ejecta mass, $\mathcal{A}$ increases with the density of the circumstellar gas of the supernova remnant because the expansion and dilution of the ejecta are slowed down for higher $n_{\rm H0}$ (i.e., $v_{\rm b}$ and $R_{\rm b}$ are smaller at the same time). An increase of the ratio $\mathcal{A}$ can also be seen when the explosion energy becomes larger but all other parameters are kept constant. The opposite trend is visible if the explosion energy and ambient density are fixed, in which case the ratio $\mathcal{A}$ decreases with larger ejecta mass. Although the blast-wave velocity at the present time is higher, it was lower early after the explosion and therefore the blast-wave radius is smaller for the larger ejecta mass.

Table 1. Illustration of the variability of the ^{44}Ti radioactivity ratios $\mathcal{A}$ as defined by Eq. (12) with different values of the model parameters. The tabulated results are at the time (age) of 320 y after the explosion for an explosion energy of $E_{\rm ej} = 1 \times 10^{51}$ erg and various combinations of values for the ejecta mass $M_{\rm ej}$, the hydrogen number density in the ambient medium, $n_{\rm H0}$, the over-density factor of the clumps, $\alpha_{\rm clmp}$, and the lower and the upper boundaries q_0 and q_1 of the mass shell where the clumps are assumed to exist. $R_{\rm b}$ and $v_{\rm b}$ are the radius and velocity of the blast-wave at that time as computed from the McKee & Truelove (1995) model for the given sets of $E_{\rm ej}$, $M_{\rm ej}$ and $n_{\rm H0}$ values

$M_{\rm ej}$ ($M_\odot$)	$n_{\rm H0}$ (cm^{-3})	$R_{\rm b}$ (pc)	$v_{\rm b}$ (10^3 km/s)	$\alpha_{\rm clmp}$	q_0	q_1	$\mathcal{A}$
2	15	1.71	2.53	5	0.4	0.6	1.47
2	15	1.71	2.53	10	0.0	0.5	1.12
2	15	1.71	2.53	10	0.4	0.6	1.55
2	15	1.71	2.53	10	0.2	0.8	1.27
2	15	1.71	2.53	20	0.4	0.6	1.34
2	30	1.51	2.15	5	0.4	0.6	1.92
2	30	1.51	2.15	10	0.0	0.5	1.30
2	30	1.51	2.15	10	0.4	0.6	1.77
2	30	1.51	2.15	10	0.2	0.8	1.43
2	30	1.51	2.15	20	0.4	0.6	1.35
3	15	1.65	2.66	5	0.4	0.6	1.27
3	15	1.65	2.66	10	0.0	0.5	1.04
3	15	1.65	2.66	10	0.4	0.6	1.27
3	15	1.65	2.66	10	0.2	0.8	1.13
3	15	1.65	2.66	20	0.4	0.6	1.18
3	30	1.47	2.23	5	0.4	0.6	1.55
3	30	1.47	2.23	10	0.0	0.5	1.13
3	30	1.47	2.23	10	0.4	0.6	1.38
3	30	1.47	2.23	10	0.2	0.8	1.22
3	30	1.47	2.23	20	0.4	0.6	1.20
4	15	1.59	2.80	5	0.4	0.6	1.14
4	15	1.59	2.80	10	0.0	0.5	1.00
4	15	1.59	2.80	10	0.4	0.6	1.15
4	15	1.59	2.80	10	0.2	0.8	1.06
4	15	1.59	2.80	20	0.4	0.6	1.11
4	30	1.43	2.32	5	0.4	0.6	1.33
4	30	1.43	2.32	10	0.0	0.5	1.05
4	30	1.43	2.32	10	0.4	0.6	1.22
4	30	1.43	2.32	10	0.2	0.8	1.12
4	30	1.43	2.32	20	0.4	0.6	1.15
5	15	1.54	2.95	5	0.4	0.6	1.07
5	15	1.54	2.95	10	0.0	0.5	0.99
5	15	1.54	2.95	10	0.4	0.6	1.08
5	15	1.54	2.95	10	0.2	0.8	1.03
5	15	1.54	2.95	20	0.4	0.6	1.07
5	30	1.40	2.41	5	0.4	0.6	1.20
5	30	1.40	2.41	10	0.0	0.5	1.01
5	30	1.40	2.41	10	0.4	0.6	1.14
5	30	1.40	2.41	10	0.2	0.8	1.07
5	30	1.40	2.41	20	0.4	0.6	1.11

Table 2. Same as Table 1 but for $E_{\rm ej} = 2 \times 10^{51}$ erg

$M_{\rm ej}$ ($\rm M_\odot$)	$n_{\rm H0}$ ($\rm cm^{-3}$)	$R_{\rm b}$ (pc)	$v_{\rm b}$ (10^3 km/s)	$\alpha_{\rm clmp}$	q_0	q_1	$\mathcal{A}$
2	5	2.44	3.63	5	0.4	0.6	1.19
2	5	2.44	3.63	10	0.0	0.5	1.03
2	5	2.44	3.63	10	0.4	0.6	1.33
2	5	2.44	3.63	10	0.2	0.8	1.26
2	5	2.44	3.63	20	0.4	0.6	1.51
2	15	2.01	2.80	5	0.4	0.6	1.53
2	15	2.01	2.80	10	0.0	0.5	1.14
2	15	2.01	2.80	10	0.4	0.6	2.07
2	15	2.01	2.80	10	0.2	0.8	1.53
2	15	2.01	2.80	20	0.4	0.6	2.03
2	30	1.77	2.40	5	0.4	0.6	2.12
2	30	1.77	2.40	10	0.0	0.5	1.36
2	30	1.77	2.40	10	0.4	0.6	2.67
2	30	1.77	2.40	10	0.2	0.8	1.76
2	30	1.77	2.40	20	0.4	0.6	2.11
3	15	1.96	2.90	5	0.4	0.6	1.47
3	15	1.96	2.90	10	0.0	0.5	1.09
3	15	1.96	2.90	10	0.4	0.6	1.74
3	15	1.96	2.90	10	0.2	0.8	1.33
3	15	1.96	2.90	20	0.4	0.6	1.54
3	30	1.74	2.46	5	0.4	0.6	2.04
3	30	1.74	2.46	10	0.0	0.5	1.30
3	30	1.74	2.46	10	0.4	0.6	2.13
3	30	1.74	2.46	10	0.2	0.8	1.53
3	30	1.74	2.46	20	0.4	0.6	1.57
4	15	1.92	3.00	5	0.4	0.6	1.36
4	15	1.92	3.00	10	0.0	0.5	1.04
4	15	1.92	3.00	10	0.4	0.6	1.48
4	15	1.92	3.00	10	0.2	0.8	1.20
4	15	1.92	3.00	20	0.4	0.6	1.31
4	30	1.71	2.53	5	0.4	0.6	1.82
4	30	1.71	2.53	10	0.0	0.5	1.20
4	30	1.71	2.53	10	0.4	0.6	1.74
4	30	1.71	2.53	10	0.2	0.8	1.36
4	30	1.71	2.53	20	0.4	0.6	1.35
5	15	1.87	3.10	5	0.4	0.6	1.25
5	15	1.87	3.10	10	0.0	0.5	1.01
5	15	1.87	3.10	10	0.4	0.6	1.31
5	15	1.87	3.10	10	0.2	0.8	1.12
5	15	1.87	3.10	20	0.4	0.6	1.20
5	30	1.68	2.59	5	0.4	0.6	1.61
5	30	1.68	2.59	10	0.0	0.5	1.11
5	30	1.68	2.59	10	0.4	0.6	1.49
5	30	1.68	2.59	10	0.2	0.8	1.23
5	30	1.68	2.59	20	0.4	0.6	1.24

Table 3. Same as Table 1 but for $E_{\rm ej} = 3 \times 10^{51}$ erg

$M_{\rm ej}$ ($\rm M_\odot$)	$n_{\rm H0}$ ($\rm cm^{-3}$)	$R_{\rm b}$ (pc)	$v_{\rm b}$ (10^3 km/s)	$\alpha_{\rm clmp}$	q_0	q_1	$\mathcal{A}$
2	5	2.68	3.84	5	0.4	0.6	1.22
2	5	2.68	3.84	10	0.0	0.5	1.04
2	5	2.68	3.84	10	0.4	0.6	1.36
2	5	2.68	3.84	10	0.2	0.8	1.36
2	5	2.68	3.84	20	0.4	0.6	1.70
2	15	2.20	3.00	5	0.4	0.6	1.44
2	15	2.20	3.00	10	0.0	0.5	1.09
2	15	2.20	3.00	10	0.4	0.6	2.13
2	15	2.20	3.00	10	0.2	0.8	1.66
2	15	2.20	3.00	20	0.4	0.6	2.57
2	30	1.93	2.57	5	0.4	0.6	1.87
2	30	1.93	2.57	10	0.0	0.5	1.22
2	30	1.93	2.57	10	0.4	0.6	2.85
2	30	1.93	2.57	10	0.2	0.8	1.87
2	30	1.93	2.57	20	0.4	0.6	2.77
3	15	2.16	3.08	5	0.4	0.6	1.47
3	15	2.16	3.08	10	0.0	0.5	1.09
3	15	2.16	3.08	10	0.4	0.6	2.01
3	15	2.16	3.08	10	0.2	0.8	1.49
3	15	2.16	3.08	20	0.4	0.6	2.01
3	30	1.90	2.63	5	0.4	0.6	2.07
3	30	1.90	2.63	10	0.0	0.5	1.30
3	30	1.90	2.63	10	0.4	0.6	2.63
3	30	1.90	2.63	10	0.2	0.8	1.72
3	30	1.90	2.63	20	0.4	0.6	2.12
4	15	2.12	3.16	5	0.4	0.6	1.42
4	15	2.12	3.16	10	0.0	0.5	1.06
4	15	2.12	3.16	10	0.4	0.6	1.78
4	15	2.12	3.16	10	0.2	0.8	1.34
4	15	2.12	3.16	20	0.4	0.6	1.64
4	30	1.88	2.68	5	0.4	0.6	2.02
4	30	1.88	2.68	10	0.0	0.5	1.26
4	30	1.88	2.68	10	0.4	0.6	2.26
4	30	1.88	2.68	10	0.2	0.8	1.55
4	30	1.88	2.68	20	0.4	0.6	1.71
5	15	2.08	3.24	5	0.4	0.6	1.35
5	15	2.08	3.24	10	0.0	0.5	1.02
5	15	2.08	3.24	10	0.4	0.6	1.57
5	15	2.08	3.24	10	0.2	0.8	1.24
5	15	2.08	3.24	20	0.4	0.6	1.42
5	30	1.85	2.74	5	0.4	0.6	1.88
5	30	1.85	2.74	10	0.0	0.5	1.19
5	30	1.85	2.74	10	0.4	0.6	1.94
5	30	1.85	2.74	10	0.2	0.8	1.41
5	30	1.85	2.74	20	0.4	0.6	1.47

It is not easy to give simple explanations for these trends. The ratio $\mathcal{A}$, which scales with the current abundance of ^{44}Ti and its effective decay rate, reflects the whole time evolution of the remnant and contains contributions from all parts of the shocked ejecta with their different ionization histories. The nonlinear dependence of $\mathcal{A}$ on the remnant parameters is a result of the interplay between a number of effects. For example, the post-shock density and temperature in the ejecta, in particular in the clumps, are important for the degree of ionization. The time when the reverse shock hits the clumps determines the time left for the equilibration between electrons and ions and for the duration of the delay of the ^{44}Ti decay. This delay lasts from the moment of nearly complete ionization until recombination takes place again.

In order to obtain a large effect on the ^{44}Ti radioactivity that is measured in Cas A presently, a high post-shock density and temperature are favorable for efficient ionization of ^{44}Ti. On the other hand, the present-day γ-ray emission of Cas A means that the temperature must not have decreased too slowly and the density not too rapidly. If that happened, ^{44}Ti would be hindered from recombination and the observed γ-ray emission could not be explained. The maximum effect from the delayed decay of ionized ^{44}Ti is found if most of the ^{44}Ti-carrying clumps have been mixed roughly half-way into the ejecta, i.e., if they are assumed to be located in the q-interval between 0.4 and 0.6 (compare Fig. 2), and if the density enhancement in the clumps is around 10 for the higher explosion energies of $E_{\rm ej} = 2 \times 10^{51}$ erg and 3×10^{51} erg (Tables 2 and 3, respectively). In case of the lowest considered value of the explosion energy, $E_{\rm ej} = 1 \times 10^{51}$ erg (Table 1), a clump over-density of about 5 seems preferable because of the higher density of the more slowly expanding ejecta. Higher than optimum $\alpha_{\rm clmp}$-values do not ensure rapid and strong ionization, whereas smaller than optimum $\alpha_{\rm clmp}$-values do not allow for quick recombination so that the decay rate stays low. If ^{44}Ti is located very far out in the remnant (large q), the temperature behind the reverse shock is too low for efficient ionization (see Fig. 1). If ^{44}Ti sits deep inside the ejecta (small q), the clumps have been reached by the reverse shock not sufficiently long ago so as to show a significant effect from ^{44}Ti ionization.

We found maximum values of $\mathcal{A}$ between roughly 1.5 and 2.5 for a large number of different combinations of remnant parameters and assumed clump locations and density enhancement factors. This means that the present-day ^{44}Ti radioactivity of Cas A could be 50% up to more than a factor of 2 higher for a certain amount of ^{44}Ti, if the decay half-life of ^{44}Ti was stretched by ionization effects. Or, reversely, the current γ-ray emission of Cas A due to ^{44}Ti decay might be explained with a significantly lower production of this nucleus during the supernova explosion. Figure 4 shows that the relative effect from the retardation of the ^{44}Ti decay will increase with the age of the remnant.

For the different considered combinations of parameter values, Cas A has reached slightly different stages of the remnant evolution around the transition time from the ejecta-dominated to the Sedov-Taylor phase. The tabulated blast-wave radius and velocity can be compared with observations which give values for the circumstellar density of about 20 hydrogen atoms per cm^3, an estimated ejecta mass of about $(2 \sim 5)\,{\rm M}_\odot$ and a blast-wave radius of 2–3 pc at a distance of 3.4 kpc (see references given in Sect. 2).

5. Summary

We examined the effects of the reverse shock on the ^{44}Ti β-decay rate in young supernova remnants. For this purpose, we employed the analytic remnant model of McKee & Truelove (1995), which was used to describe the hydrodynamic evolution. We assumed that ^{44}Ti is carried by ^{56}Fe-dominated, dense clumps which are mixed into the otherwise homogeneous supernova ejecta and account for a minor fraction of the ejecta mass. Strong ionization of ^{44}Ti due to the heating by the reverse shock and a sizable influence on the ^{44}Ti decay is obtained if the clumps are assumed to be located at intermediate values of the radial mass coordinate q. The observationally important change of the ^{44}Ti decay activity, however, depends also on the values of the remnant parameters, namely the explosion energy, the ejecta mass, the density of the ambient medium and the assumed overdensity factor of the clumps relative to the embedding homogeneous ejecta.

We applied our model to the case of Cas A, a young supernova remnant with an age of about 320 years. Observational data are considered to constrain the parameter space which was explored. We found that under certain conditions the ionization of ^{44}Ti and the corresponding delay of its decay can yield an up to three times higher ^{44}Ti activity at the present time than predicted on the grounds of the laboratory decay rate. This effect is large enough to reduce the apparent discrepancies between the ^{44}Ti production in the explosion as inferred from the COMPTEL γ-line measurements and the theoretical expectations from the current supernova nucleosynthesis models.

We emphasize again that to get an enhanced ^{44}Ti decay activity we had to assume ^{44}Ti to be associated with inhomogeneities in the ejecta which contain the Fe-group elements. Hydrodynamical models have so far not been able to predict the fraction of Fe and ^{44}Ti in such clumpy structures, the overdensity of the clumps relative to the surrounding material at the considered age of a supernova remnant, the dynamics of the clumps, and their size and distribution. Multi-dimensional supernova models are called for, which connect the very early phase of the explosion with the remnant evolution a few hundred years

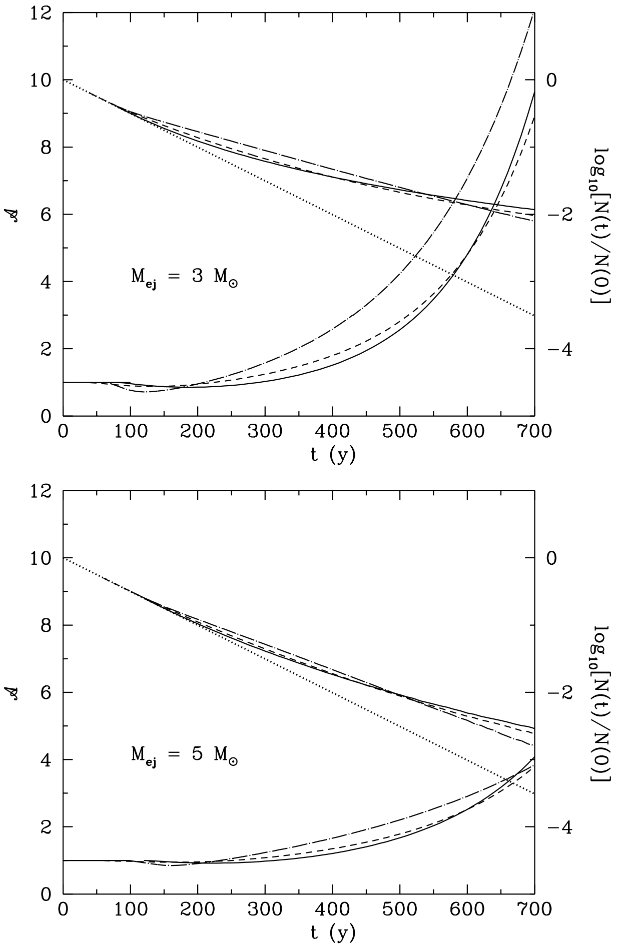

Fig. 4. The decrease with time of the amount of ^{44}Ti in the supernova remnant, $N(t)$, by β-decays, starting from the initial amount $N(0)$ (*right scale* in logarithm), and the corresponding, mostly increasing activity ratio $\mathcal{A}$ (*left scale*). Values of 3 $M_\odot$ (*upper panel*) and 5 $M_\odot$ (*lower*) are used for M_{ej}, while $E_{ej} = 2 \times 10^{51}$ erg, $n_{H0} = 15$ cm^{-3} and $\alpha_{clmp} = 10$ are adopted in both cases. The different lines show results obtained for different assumptions of the radial locations of the clumps: $q = [q_0, q_1] = [0.0, 0.5]$ (*solid line*), [0.4, 0.6] (*dash-dotted line*), and [0.2, 0.8] (*dashed line*). The exponential decrease of the ^{44}Ti abundance with the laboratory rate is plotted by the *dotted line*

later. Self-consistent multi-dimensional simulations have yet to be carried out for an improved theoretical picture of the explosive ^{44}Ti production in supernovae. All published theoretical yields have so far only been obtained with ad-hoc assumptions, most often by spherically symmetric models and/or simulations of the supernova explosions which were started from artificial initial conditions ("piston" models) rather than self-consistent situations. We add that such calculations also suffer from uncertainties concerning the nuclear reaction rates which are important to determine the ^{44}Ti yield (The et al. 1998).

On the other hand, more detailed X-ray and γ-ray observations with a better spatial (and energy) resolution are desirable to confirm or reject the implications of the described model, e.g., the existence of Fe-containing knots with temperatures in the approximate range of ($1 \sim 5$) keV (cf. Tsunemi 1997). The current angular resolution of the ASCA/SIS observations, about one arcmin, is insufficient to measure the thermodynamic properties of individual clumps in the ejecta of Cas A. Only information is available for the average electron temperature in the matter that is heated by the forward and reverse shocks. Comparing the observations with predictions from the remnant model used in this paper would therefore require monitoring of the thermodynamic history of the homogeneous ejecta. For this, one would need to compute the thermal state of the electrons, and would have to specify the unknown composition of the ejecta, which is very uncertain because it depends on the type of progenitor and explosion. The described investigations of ^{44}Ti decay in supernova remnants could be done without such additional assumptions, but the models do not provide a description of the thermodynamic state of the remnant, which allows for a direct comparison with current observational data.

Finally, we mention that we applied our analysis also to the new supernova remnant, RX J0852.0-4622, discovered in the direction of the Vela remnant by Aschenbach (1998), in which a source of ^{44}Ti line emission has been detected (Iyudin et al. 1998). However, for the estimated low density of the ambient medium of less than $0.04(d/500\text{pc})^{-0.5}$ cm^{-3} with a distance d to the remnant (Aschenbach 1998), we found that the reverse shock does not heat the ejecta to sufficiently high temperatures to ionize ^{44}Ti.

Acknowledgements. We thank H. Tsunemi, J. Vink, E. Miyata and K. Nomoto for helpful information and discussions. This work was supported by the SFB-375 "Astroparticle Physics" of the Deutsche Forschungsgemeinschaft.

Appendix A: reaction rates and related uncertainties

We estimate here the β-decay, ionization and recombination rates, which appear in Eq. (7). We also evaluate their uncertainties in relation to the results presented in Sect. 4.

The orbital-electron capture rate of ^{44}Ti: We first formulate the β-decay rate of (near) neutral ^{44}Ti. The corresponding half-life $t_{1/2}$ has been well determined to be 60 y (Ahmad et al. 1998; Görres et al. 1998; Norman et al. 1998; Wietfeldt et al. 1999). The ^{44}Ti β-decay is by orbital-electron capture almost exclusively to the 146 keV excited (0^-) state of ^{44}Sc (Endt 1998), the corresponding Q-value being 266 keV. We thus write the laboratory rate, $\lambda_{lab} = \ln 2/t_{1/2}$, as

$$\lambda_{lab} = \lambda_K + \lambda_{LI} + ... \quad (13)$$

where $\lambda_{\rm K}, \lambda_{\rm LI}$ etc. refer to the rates for partial captures of K ($1s_{\frac{1}{2}}$), LI ($2s_{\frac{1}{2}}$) electrons etc. In the "normal" approximation (e.g. Konopinski & Rose 1965), $\lambda_{\rm K}$ for example reads

$$\lambda_{\rm K} = \frac{G_{\rm A}^2}{4\pi^2}|M_0|^2(Q + B_{\rm K})^2 g_{\rm K}^2 \,, \tag{14}$$

for the transition of our current interest, where $G_{\rm A}$ is the axial-vector coupling constant of weak interaction, M_0 is a linear combination of two major nuclear matrix elements in the rank-0 first-forbidden ($0^+ \to 0^-$) transition, Q is the Q-value, and $B_{\rm K}$ is the binding energy of the K-shell. Thus, $q_\nu \equiv Q + B_{\rm K}$ is the energy available to the emitted neutrino. (The nuclear recoil energy is very small and is ignored here.) Finally, $g_{\rm K}$ is the larger component of the radial wave-functions of the K-electron, which is evaluated at the nuclear radius.

Since Q is much larger than the binding energies (about 5 keV for K-electrons), the relative ratios of the partial decay rates become nearly equal to those of the respective wave-functions squared. Considering in addition that αZ is not very large, we have

$$\lambda_{\rm LI} \approx \frac{1}{8}\lambda_{\rm K} \,, \tag{15}$$

since $g_{\rm LI}^2 \approx g_{\rm K}^2/8$ in the low-αZ approximation. With the use of the same approximation, one finds that the capture rates of the higher-shell electrons are small.

Correspondingly, the orbital-electron capture rates of ^{44}Ti with i orbital electrons [i.e., (22-i)-times ionized] are approximately given by

$$\lambda_{\beta,i} \approx p_{i,{\rm K}}\lambda_{i,{\rm K}} + p_{i,{\rm LI}}\lambda_{i,{\rm LI}} \,, \tag{16}$$

where $p_{i,{\rm K}}$ and $p_{i,{\rm LI}}$ are the occupancies ([0,1]) of the K and $\rm L_I$ orbits, respectively, and $\lambda_{i,{\rm K}}$ and $\lambda_{i,{\rm LI}}$ are the corresponding capture rates for the *filled* shells. We approximate the partial capture rates by

$$\lambda_{i,{\rm K}} \approx \frac{8}{9}\lambda_{i,{\rm K+LI}} \approx \frac{8}{9}\lambda_{\rm lab},\ \lambda_{i,{\rm LI}} \approx \frac{1}{9}\lambda_{i,{\rm K+LI}} \approx \frac{1}{9}\lambda_{\rm lab} \,, \tag{17}$$

so that the total (effective) decay rate reads

$$\lambda_{\rm eff} \approx \Big(\frac{4}{9}n_1 + \frac{8}{9}n_2 + \frac{17}{18}n_3 + \sum_{i\ge4} n_i\Big)\lambda_{\rm lab} \Big/ \sum_{i\ge0} n_i \,, \tag{18}$$

where n_i is the number abundance of $^{44}{\rm Ti}^{+22-i}$.

The above procedure is quite well suited for dealing with the decays of highly-ionized ^{44}Ti. In fact, our calculations based on a relativistic mean field method (Libermann et al. 1971) show that the overall errors associated with those approximations, including the neglect of the decrease of screening and the slightly altered energetics along with ionization, are small enough (less than 10 %) to be ignored in the present work.

The ionization rates of ^{44}Ti *and* ^{56}Fe: The rates of electron-induced ionization are given by

$$\lambda_{{\rm ion},i} = n_{\rm e}\sum_{i\ge1}\Big(p_{i,{\rm K}}\left\langle\sigma_{{\rm ion},i}^{({\rm K})}v\right\rangle + p_{i,{\rm LI}}\left\langle\sigma_{{\rm ion},i}^{({\rm LI})}v\right\rangle + ...\Big) \,, \tag{19}$$

where $n_{\rm e}$ is the electron number density and $\langle\sigma_{{\rm ion},i}v\rangle$ is the Maxwellian-average of the cross section (times the electron velocity v) for ionization of filled K-, LI-... shell electrons. As in Eq. (16), $p_{i,{\rm K}}$ and $p_{i,{\rm LI}}$ stand for occupancies of the K- and $\rm L_I$ shells in the i-th ion. Our estimates of $\sigma_{{\rm ion},i}$ rely on the experimental data on K-shell ionization by electrons in the relevant energy range of $6-50$ keV (Long et al. 1990).

We start with the classical Bethe-Mott-Massey formula (e.g., Powell 1976), which for the K-shell ionization from an ion with i bound electrons reads

$$\sigma_{{\rm ion},i}^{({\rm K})} = [\pi{\rm e}^4/(EB_{i,{\rm K}})]Z_{\rm K}b_{i,{\rm K}}\ln[4c_{i,{\rm K}}E/B_{i,{\rm K}}] \,, \tag{20}$$

where $B_{i,{\rm K}}$ is the K-binding energy (taken positive), $E(\ge B_{i,{\rm K}})$ is the incident electron energy, and $Z_{\rm K} = 2$ is the number of K-electrons, and we treat $b_{i,{\rm K}}$ and $c_{i,{\rm K}}$ as adjustable parameters. It turns out that the existing experimental data for K-ionization of Ti by electrons in the relevant E range of 6 - 50 keV (Long et al. 1990) can be well reproduced by the choice of

$$1/c_{22,{\rm K}} \approx a + (4-a)\exp[d(E/B_{22,{\rm K}} - 1)] \,, \tag{21}$$

with $a = 0.55$, $d = 0.45$, and $b_{22,{\rm K}} = 0.445$. For simplicity, we use the same parameter values for the higher shells as well as for highly-ionized cases. Aside from the trivial replacements of $Z_{\rm K}$ by $Z_{\rm LI}$ etc., we use the binding energies computed for each ion by the relativistic formalism, because the rates are sensitive to those thresholds. For ^{44}Ti, their values in keV are, e.g., $B_{1,{\rm K}} = 6.6, B_{2,{\rm K}} = 6.2, B_{3,{\rm K}} = 6.1, B_{3,{\rm LI}} = 1.4, B_{4,{\rm K}} = 5.9, B_{4,{\rm LI}} = 1.3$, in contrast to $B_{22,{\rm K}} = 5.0, B_{22,{\rm LI}} = 0.56$.

The same parameter values also reproduce the K-shell ionization cross-section data for Ni (Long et al. 1990) within the experimental uncertainties, while slightly (up to 20 %) over-estimating the limited data points for Mn. When considered for Fe, this order of the uncertainty of the ionization rates influences the radioactivity under consideration in this work only at a negligible level.

The recombination rates of ^{44}Ti *and* ^{56}Fe: The recombination rates are given by

$$\lambda_{{\rm rec},i} = n_{\rm e}\sum_{i\ge0}\Big(q_{i,{\rm K}}\left\langle\sigma_{{\rm rec},i}^{({\rm K})}v\right\rangle + q_{i,{\rm LI}}\left\langle\sigma_{{\rm rec},i}^{({\rm LI})}v\right\rangle + ...\Big) \,, \tag{22}$$

where $q_i \equiv 1 - p_i$ are the vacancies of the respective shell prior to the recombination. We adopt the well-known formulae (Stobbe 1930) for the recombination cross-sections in the non-relativistic approximation for a pure Coulomb field. They are expressed in analytic forms in terms of the ratios of the incident electron energies ($E \geq 0$) to the binding energies of respective shells. The relativistic and screening effects can roughly be estimated with the use of effective charges, which turn out to be largely insignificant for the purpose of the present work.

References

Ahmad I., et al., 1998, Phys. Rev. Lett. 80, 2550
Anderson M. C., Rudnick L., 1995, ApJ 441, 307
Aschenbach B., 1998, Nature 396, 141
Burrows A., Hayes J., Fryxell B. A., 1995, ApJ 450, 830
Chevalier R. A., Kirshner R. P., 1977, ApJ 218, 142
Chevalier R. A., Kirshner R. P., 1978, ApJ 219, 931
Chevalier R. A., Kirshner R. P., 1979, ApJ 233, 154
Clayton D. D., The L.-S., Leising M. D., Johnson W. N., Kurfess J. D., 1992, ApJ 399, L141
Diehl R., Timmes F.X., 1998, PASP 110,637
Dupraz C., et al., 1997, A&A, 324, 683
Endt P. M., 1998, Nucl. Phys. A633, 1
Fesen R. A., Becker R. H., 1991, ApJ 371, 621
Fryxell B., Müller E., Arnett W. D., 1991 ApJ 367, 619
Görres J. et al., 1998, Phys. Rev. Lett. 80, 2554
Hanuschik R. W., Dachs J., 1987, in: *Supernova 1987A*, ed. I. J. Danziger, Garching: ESO, p. 153
Hartmann D. H., et al., 1997, Nucl. Phys. A621, 83c
Herant M., Benz W., Colgate S. A., 1992, ApJ 395, 642
Herant M., Benz W., Hix W. R., Fryer C. L. Colgate S. A., 1994, ApJ 435, 339
Holt S. S., Gotthelf E. V., Tsunemi H., Negoro H., 1994, PASJ 46, L151
Hurford A. P., Fesen, R. A., 1996, ApJ 469, 246
Iyudin A. F., et al., 1994, A&A 284, L1
Iyudin A. F., et al., 1997, ESA SP-382, 37
Iyudin A. F., et al., 1998, Nature 396, 142
Janka H.-Th., Müller E., 1995, ApJ 448, L109
Janka H.-Th., Müller E., 1996, A&A 306, 167
Jansen F., et al., 1988, ApJ 331, 949
Konopinski E.J., Rose M. E., 1965, in: *Alpha-, beta- and gamma-spectroscopy*, K. Siegbahn (ed.), Amsterdam: North Holland Pub., p. 1327
Koralesky B., Rudnik L., Gotthelf E. V., Keohane J. W., 1998, ApJ 505, L27
Kurfess J. D., et al., 1992, ApJ 399, L137
Lagage P. O., et al., 1996, A&A 315, L273
Liberman D. A., Cromer D. T., Waber J. T., 1971, Comput. Phys. Comm. 2, 107
Long X., Liu M., Ho F., Peng X., 1990, Atom. Dat. Nucl. Dat. Tables 45, 353
Mahoney W.A., et al., 1988, ApJ 334, L81
McKee C. F., Truelove J. K., 1995, Phys. Rep. 256, 157
Matz S. M., et al., 1988, Nature 331, 416
Miyata E., 1996, PhD thesis, Osaka Univ. (unpublished)
Mochizuki Y., 1999, in: *Nuclei in the cosmos V*, N. Prantzos, S. Harrissopulos (eds.), p. 285 Gif-sur-Yvette: Editions Frontières, to appear
Morris D. J., et al., 1995, N.Y. Acad. Sci. 759, 397
Morris D. J., et al., 1997, AIP Conf. Proc. 410, 1084
Nagataki S. Hashimoto M., Sato K., Yamada S., Mochizuki Y. S., 1998, ApJ 492, L45
Nomoto K., Shigeyama T., Kumagai S., Yamaoka H., Suzuki T., 1994, in: *Supernovae*, S.A. Bludman, R. Mochkovitch, J. Zinn-Justin (eds.), Amsterdam: North-Holland Pub., p. 489
Norman E. B., et al., 1998, Phys. Rev. C57, 2010
Peimbert M., van den Bergh S., 1971, ApJ 167, 223
Phillips M. M., Heathcote S. R., 1989, PASP 101, 137
Powell C. J., 1976, Rev. Mod. Phys. 48, 33
Prantzos N., Diehl R., 1996, Phys. Rep. 267, 1
Reed J. E., Hester J. J., Fabian A. C., Winkler P. F., 1995, ApJ 440, 706
Rester A. C., et al., 1988, ApJ 342, L71
Reynoso E. M., Goss W. M., Dubner G. M., Winkler P. F., Schwarz U. J., 1997, A&A 317, 203
Sandie W. G., et al., 1988, ApJ 334, L91
Sgro A. G., 1975, ApJ 197, 621
Shimizu T., 1995, Ph.D. thesis, Univ. Tokyo (unpublished)
Shimizu T., Yamada S., Sato K., 1994, ApJ 432, L119
Spitzer L. Jr., 1962, *Physics of fully ionized gases*, New York: John Wiley & Sons
Stobbe M., 1930, Ann. Physik 7, 661
Teegarden B.J., et al., 1989, Nature 339, 122
The L. S., et al., 1996, A&A S 120, 357
The L. S., Clayton D. D., Jin L., Meyer B. S., 1998, preprint astro-ph/9806211
Thielemann F.-K., Nomoto K., Hashimoto M., 1996, ApJ 460, 408
Timmes F. X., Woosley S. E., 1997, ApJ 489. 160
Timmes F. X., Woosley S. E., Hartmann D. H., Hoffman R. D., 1996, ApJ 464, 332
Tsunemi H., 1997, in: *X-ray Imaging and Spectroscopy of Cosmic Hot Plasmas*, F. Makino, K. Mitsuda (eds.), Tokyo: Universal Academy Press, p. 325
Tsunemi H., Yamashita K., Masai K., Hayakawa S., Koyama K., 1986, ApJ 306, 248
Utrobin V. P., Chugai N. N., Andronova A. A., 1995, A&A 295, 129
van den Bergh S., Kamper K., 1983, ApJ 268, 129
Vink J., Kasstra J. S., Bleeker A. M., 1996, A&A 307, L41
Wietfeldt F. E., Schima F. J., Coursey B. M., Hoppes D. D., 1999, Phys. Rev. C59, 528
Wooden D. H., 1997, in: *Astrophysical Implications of the Laboratory Study of Presolar Materials*, T. Bernatowicz, E. Zinner (eds.), New York: AIP Conference Proceedings, p. 317
Woosley S. E., Weaver T. A., 1994, in: *Supernovae*, S.A. Bludman, R. Mochkovitch, J. Zinn-Justin (eds.), Amsterdam: North-Holland Pub., p. 63
Woosley S. E., Weaver T. A., 1995, ApJS 101, 181
Woosley S. E., Arnett W. D., Clayton D. D., 1973 ApJS 26, 231
Woosley S. E., Langer N., Weaver T. A., 1995, ApJ 448, 315
Woosley S. E., Diehl R., 1998, Physics World, 11, 7, 22

This article was processed by the author using Springer-Verlag LaTeX A&A style file *L-AA* version 3.